Supporting Information

Engineering iron atom-cluster nanostructure towards efficient and durable electrocatalysis

Feng-Yi Zheng [a], Ruisong Li [b], Shibo Xi [c], Fei Ai [a], Jike Wang [a, *]

[a] *The Institute for Advanced Studies, Wuhan University, Hubei 430072, P. R. China*

[b] *State Key Laboratory of Marine Resource Utilization in South China Sea, Hainan Provincial Key Lab of Fine Chemistry, School of Chemical Engineering and Technology, Hainan University, Haikou 570228, P. R. China*

[c] *Institute of Chemical and Engineering Sciences, A*STAR (Agency for Science, Technology and Research), Singapore 627833, Singapore*

***Corresponding author**: Jike.Wang@whu.edu.cn (J. Wang)*

Table of contents

Section 1. Supporting Figures and Tables

Section 2. References

Section 1. Supporting Figures and Tables

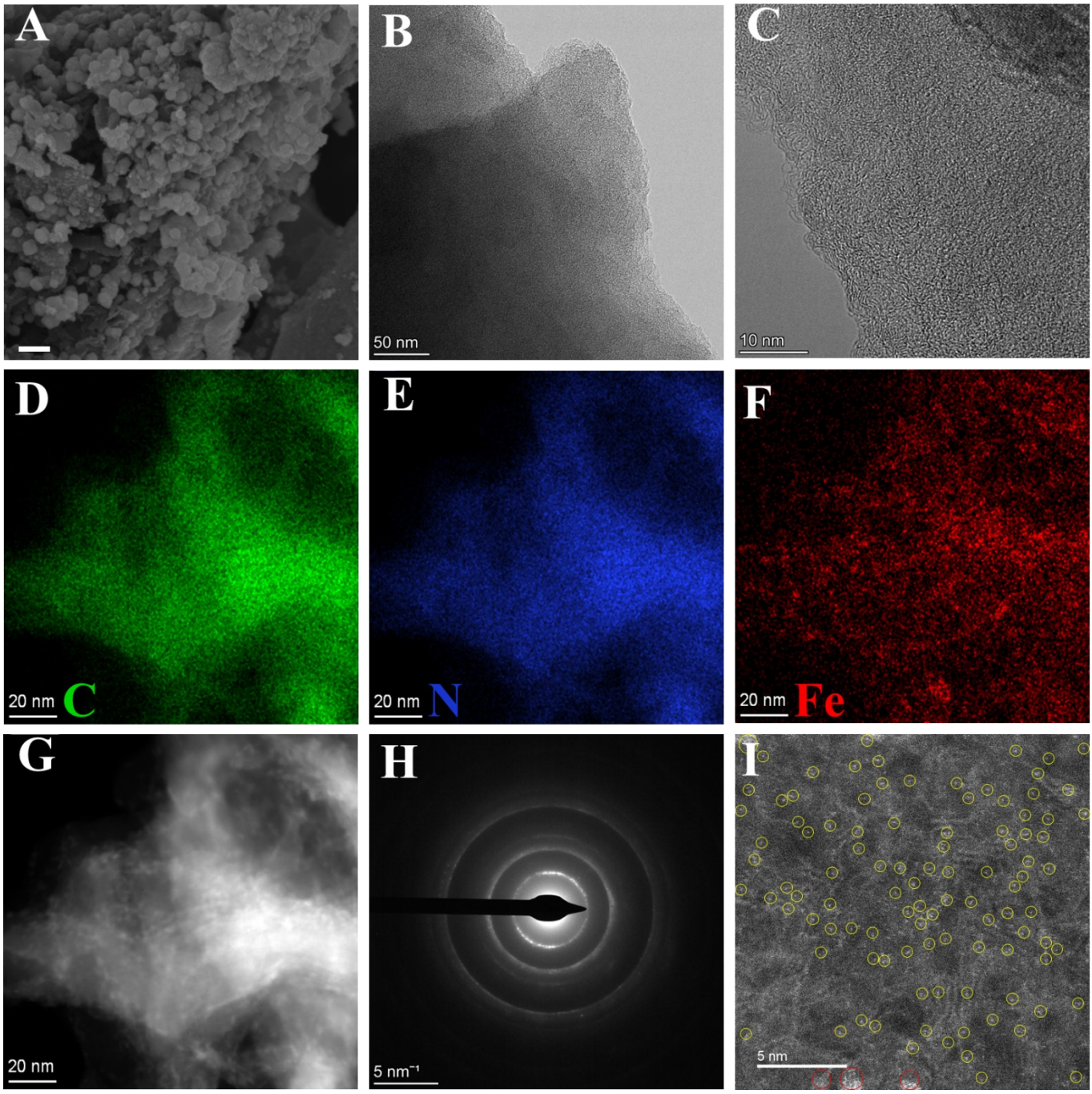

Fig. S1 A) SEM, B) TEM, C) HRTEM, G) HAADF-STEM and corresponding elemental mapping images of D) C, E) N and F) Fe elements, H) SAED, and I) aberration-corrected HAADF-STEM image (yellow circles: single atoms; red circles: clusters) of Fe_{SA}/Fe_{AC}-NC 800.

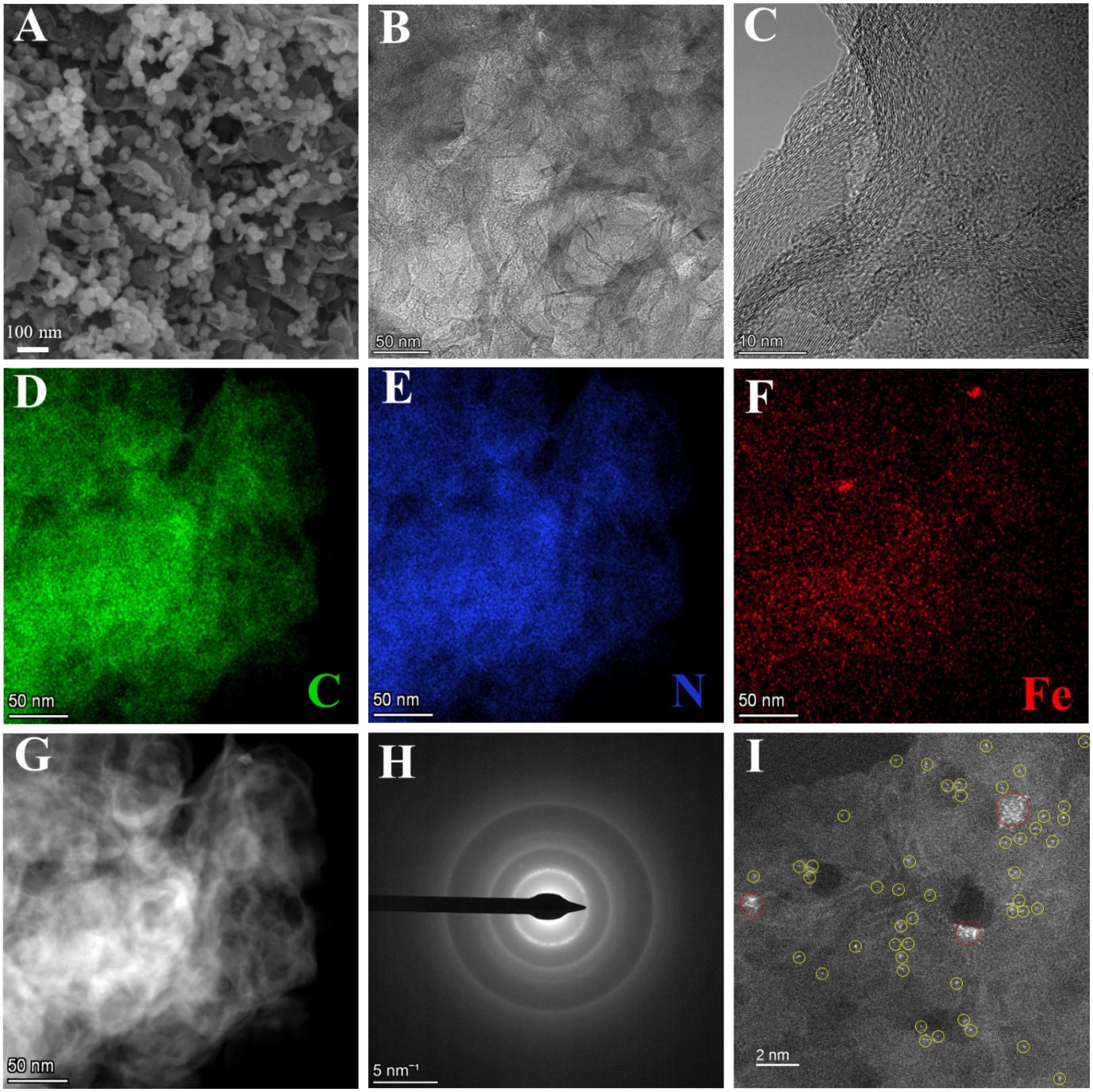

Fig. S2 A) SEM, B) TEM, C) HRTEM, G) HAADF-STEM and corresponding elemental mapping images of D) C, E) N and F) Fe elements, H) SAED, and I) aberration-corrected HAADF-STEM image (yellow circles: single atoms; red circles: clusters) of Fe_{SA}/Fe_{AC}-NC 1000.

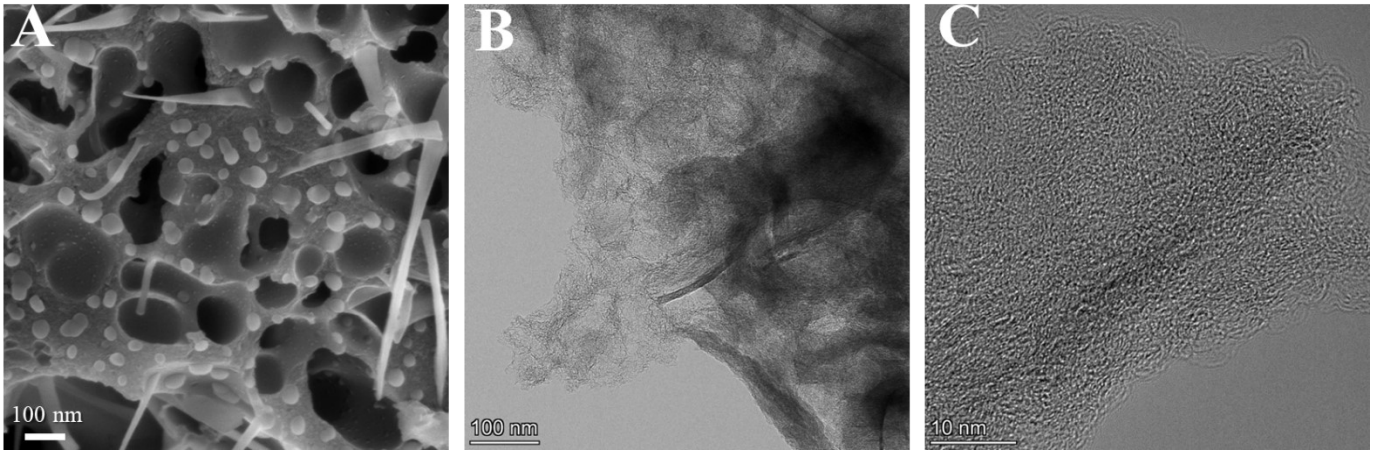

Fig. S3 A) SEM, B) TEM and C) HRTEM images of C 900.

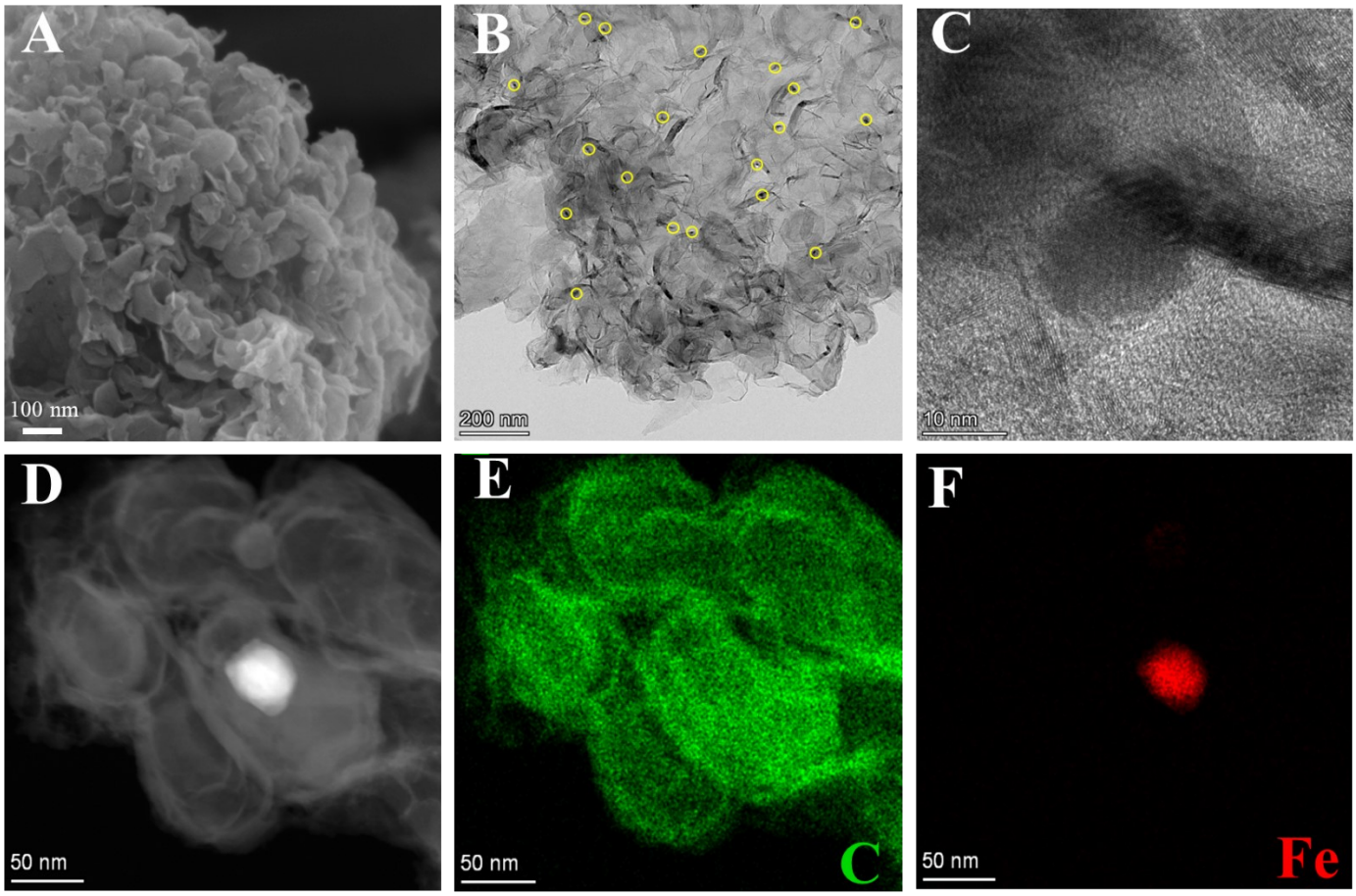

Fig. S4 A) SEM, B) TEM, C) HRTEM and D) HAADF-STEM and corresponding elemental mapping images of E) C and F) Fe elements in Fe_{AC}-C 900. In B), the yellow circles indicate the Fe micro-clusters of the carbon framework.

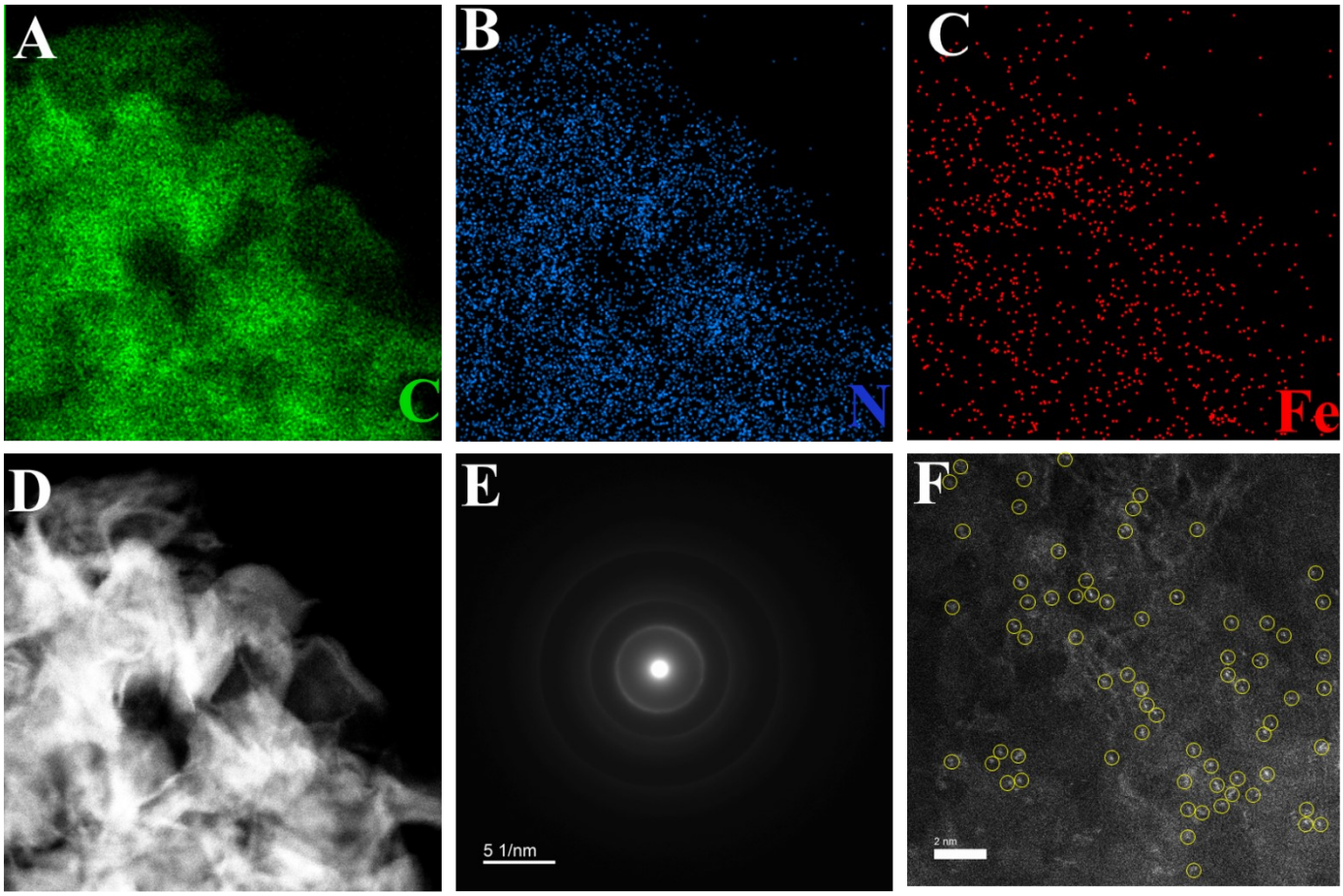

Fig. S5 D) HAADF-STEM and corresponding elemental mapping images of A) C, B) N and C) Fe elements, E) SAED, and F) aberration-corrected HAADF-STEM image (yellow circles: single atoms) of Fe_{SA}-NC 900.

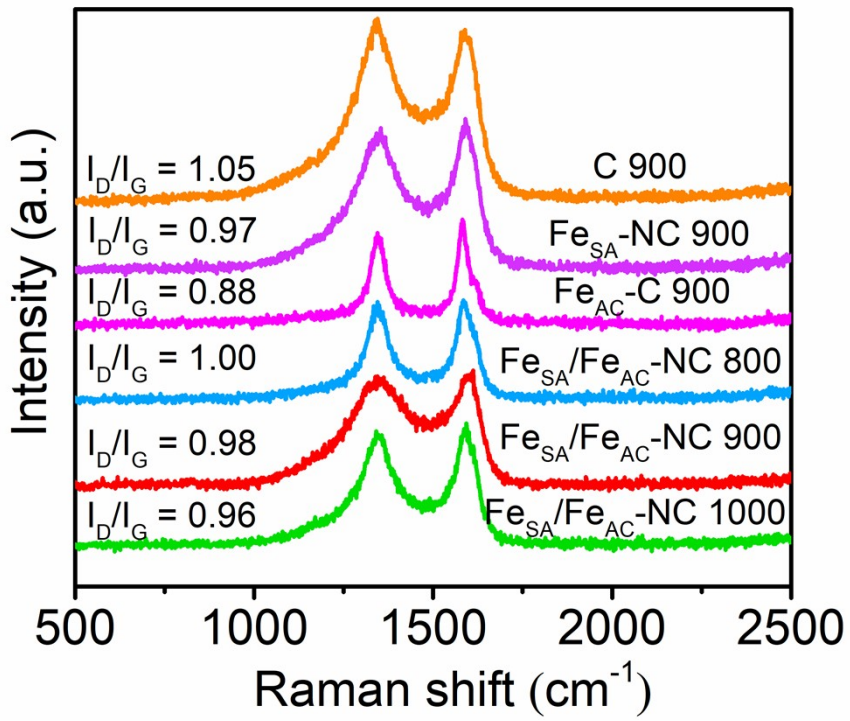

Fig. S6 Raman scattering patterns of electrocatalysts.

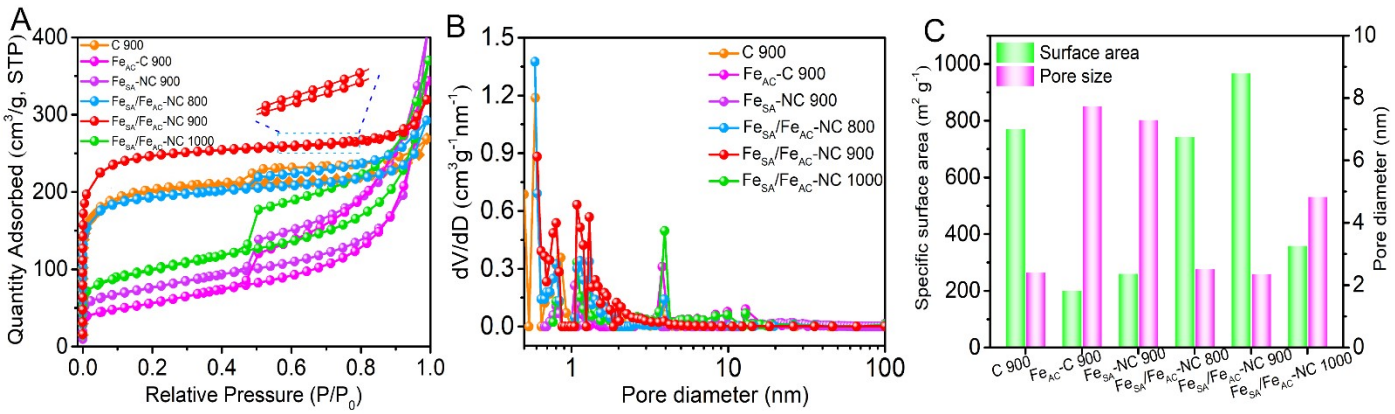

Fig. S7 A) N_2 adsorption/desorption isotherms, B) pore diameter distributions, C) BET pore widths and specific surface areas of electrocatalysts.

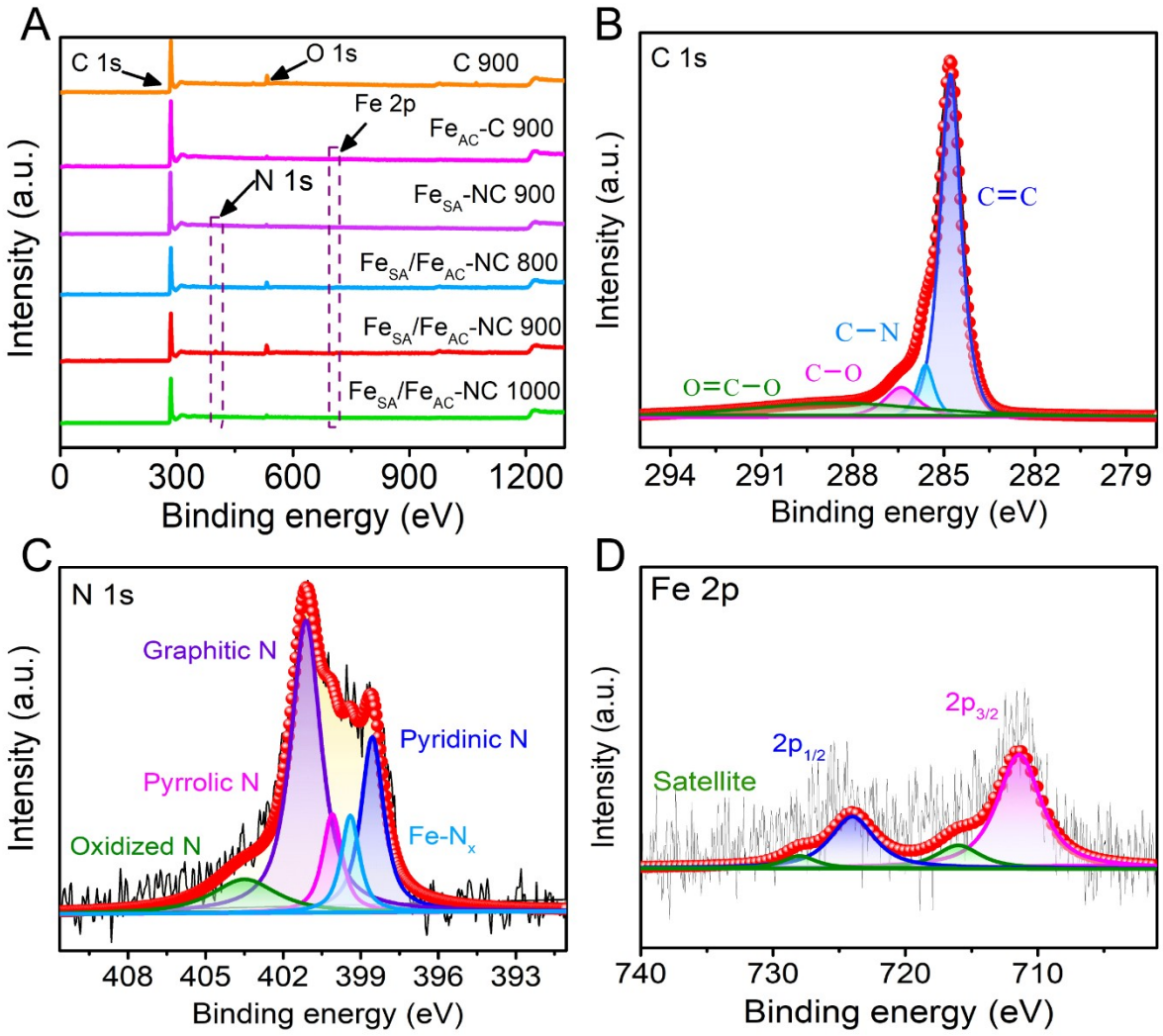

Fig. S8 A) XPS survey spectra of electrocatalysts. B) High-resolution C 1s, C) N 1s, and D) Fe 2p spectra of Fe_{SA}/Fe_{AC}-NC 900.

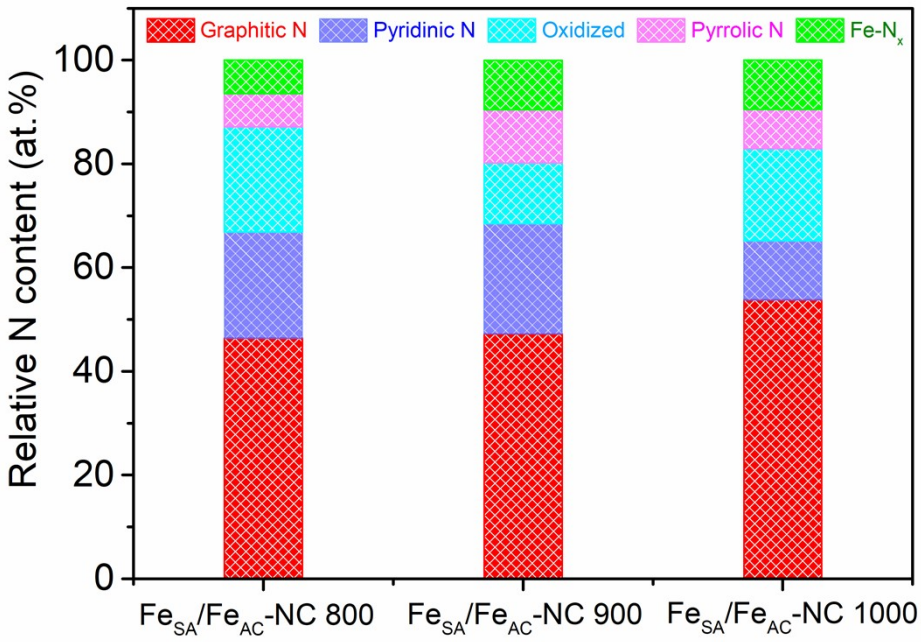

Fig. S9 The contents of different N species of Fe_{SA}/Fe_{AC}-NCs catalysts.

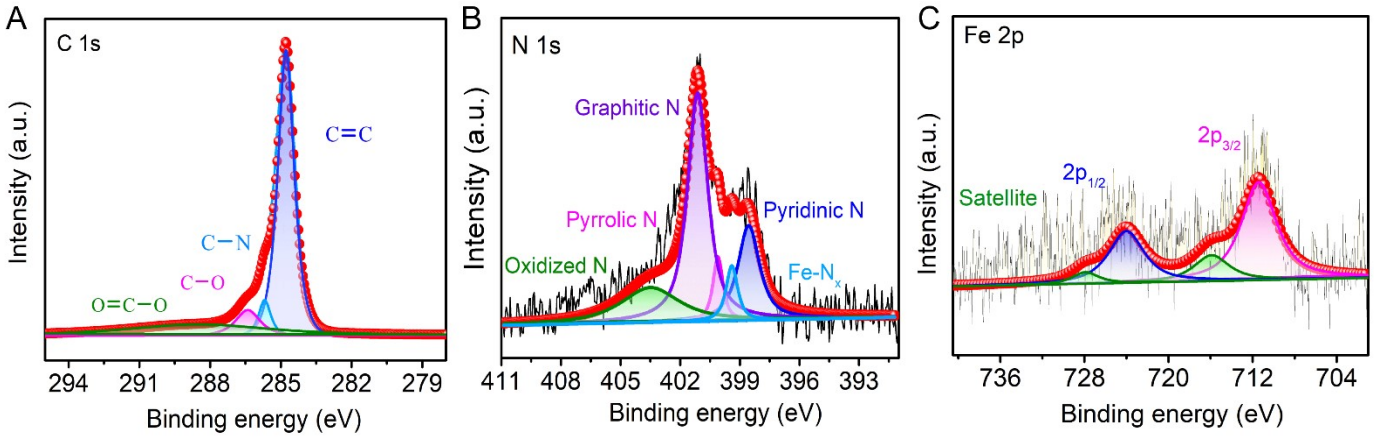

Fig. S10 A) High-resolution C 1s spectra, B) N 1s spectra and C) Fe 2p spectra of Fe_{SA}/Fe_{AC}-NC 800.

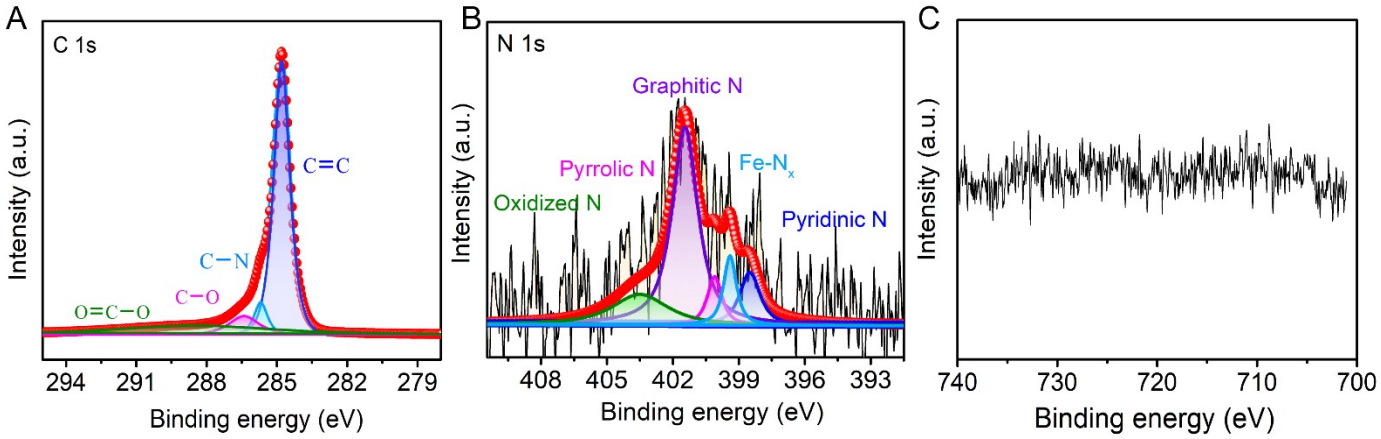

Fig. S11 A) High-resolution C 1s spectra, B) N 1s spectra and C) Fe 2p spectra of Fe_{SA}/Fe_{AC}-NC 1000.

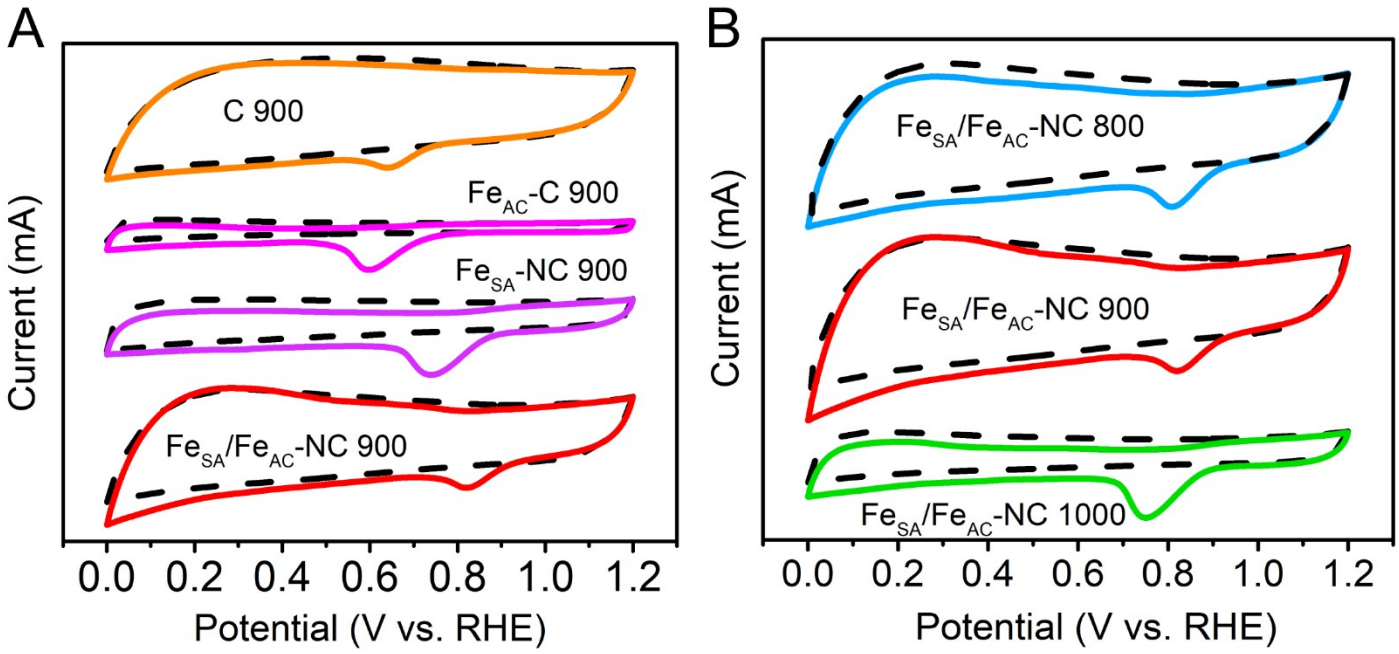

Fig. S12 CV curves for A) catalysts based on doping source and B) catalysts based on pyrolysis temperature in N_2-saturated (dash line) and O_2-saturated (solid line) 0.1 M KOH electrolyte.

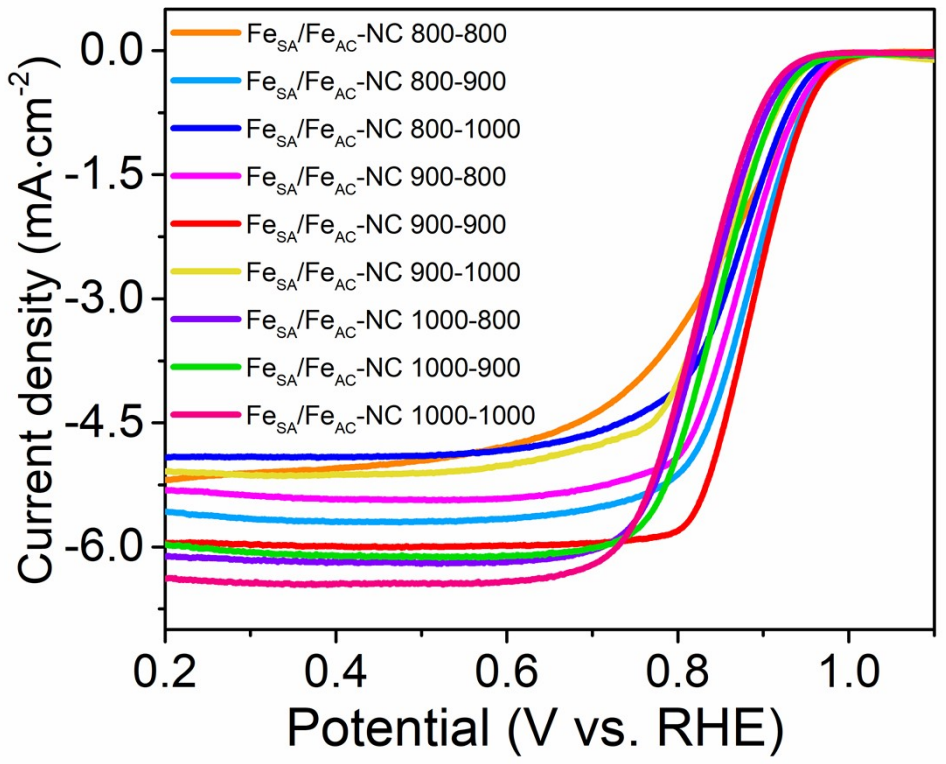

Fig. S13 ORR polarization curves of Fe_{SA}/Fe_{AC}-NCs electrocatalysts that are manufactured under different pyrolysis temperatures.

We first annealed the Fe_{SA}/Fe_{AC}-NC precursors from 800 to 1000 ℃. After acid etching, the acquired product was carbonized again from 800 to 1000 ℃. And the final catalyst was denoted as Fe_{SA}/Fe_{AC}-NC-a-b, where a was the first pyrolysis temperature and b was the second pyrolysis temperature. The ORR polarization properties of all obtained samples were evaluated in an O_2-saturated 0.1 M KOH aqueous resolution.

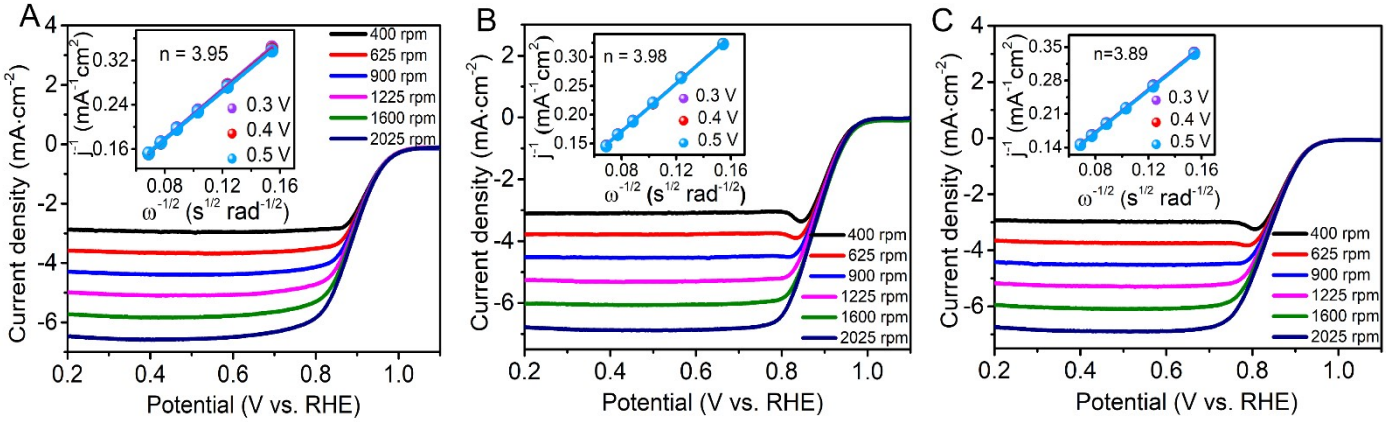

Fig. S14 LSV polarization curves of the Fe_{SA}/Fe_{AC}-NC 800 A), Fe_{SA}/Fe_{AC}-NC 900 B) and Fe_{SA}/Fe_{AC}-NC 1000 C) catalysts in an O_2-saturated 0.1 M KOH aqueous solution at a sweep rate of 5 mV s^{-1} with different rotation rates (400-2025 rpm) and the corresponding K-L plots (j^{-1} versus $\omega^{-1/2}$) at different potentials (inset).

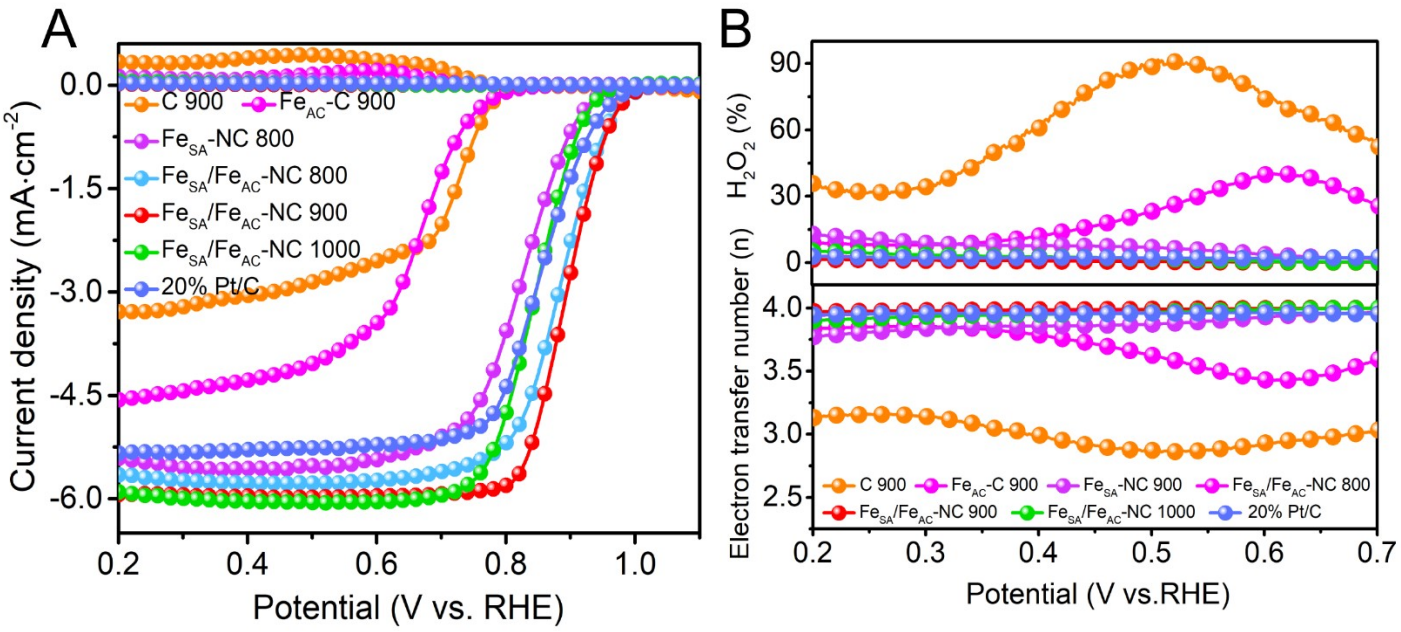

Fig. S15 A) Disk and ring current, B) electron transfer number (n) and H_2O_2 yield for various catalysts at 1600 rpm in alkaline media.

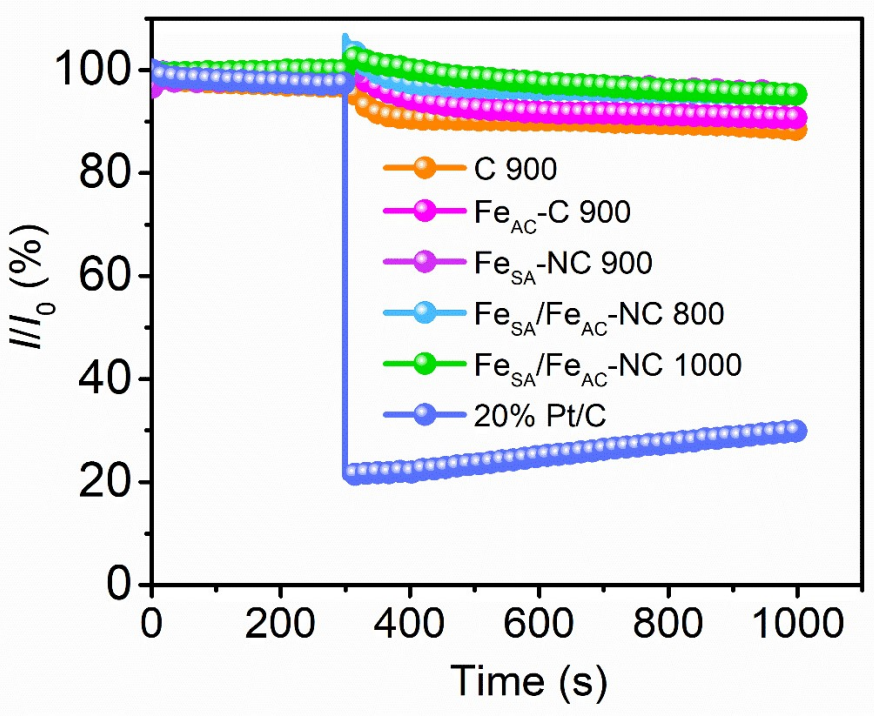

Fig. S16 *I-t* CA responses for various catalysts at 0.6 V and 1600 rpm with 3M methanol addition at around 300s in 0.1 M KOH. I_0 defined the initial current.

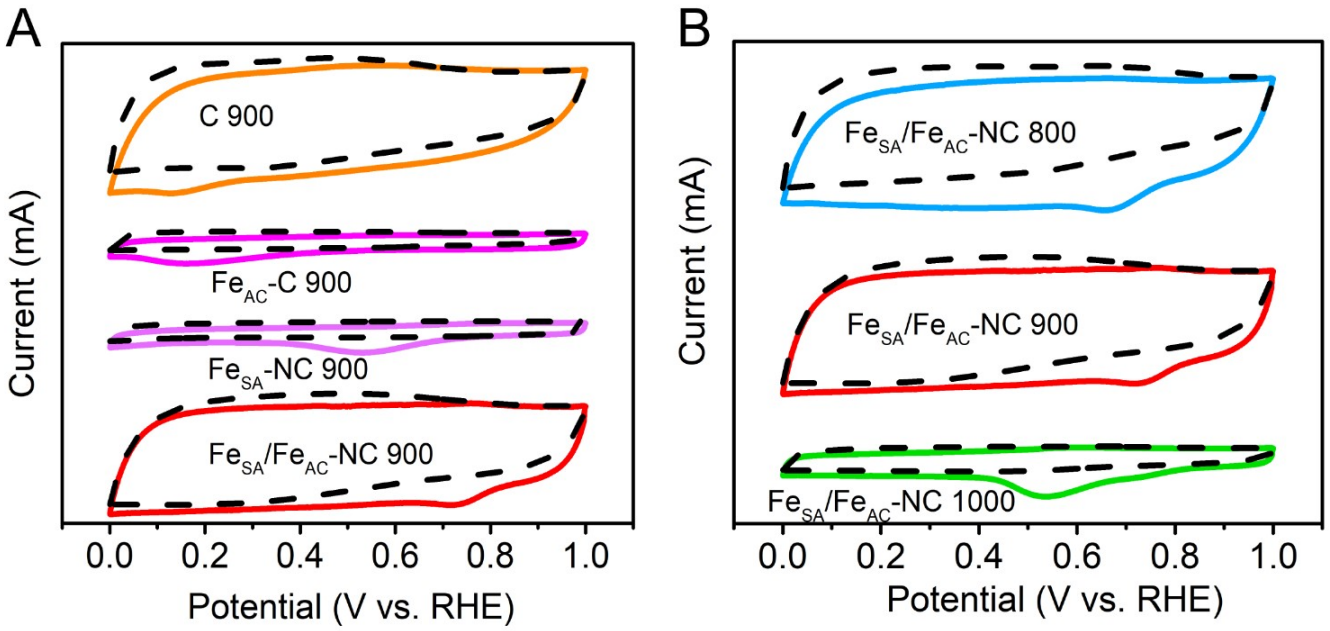

Fig. S17 CV curves for A) catalysts based on doping source and B) catalysts based on pyrolysis temperature in N_2-saturated (dash line) and O_2-saturated (solid line) 0.1 M $HClO_4$ electrolyte.

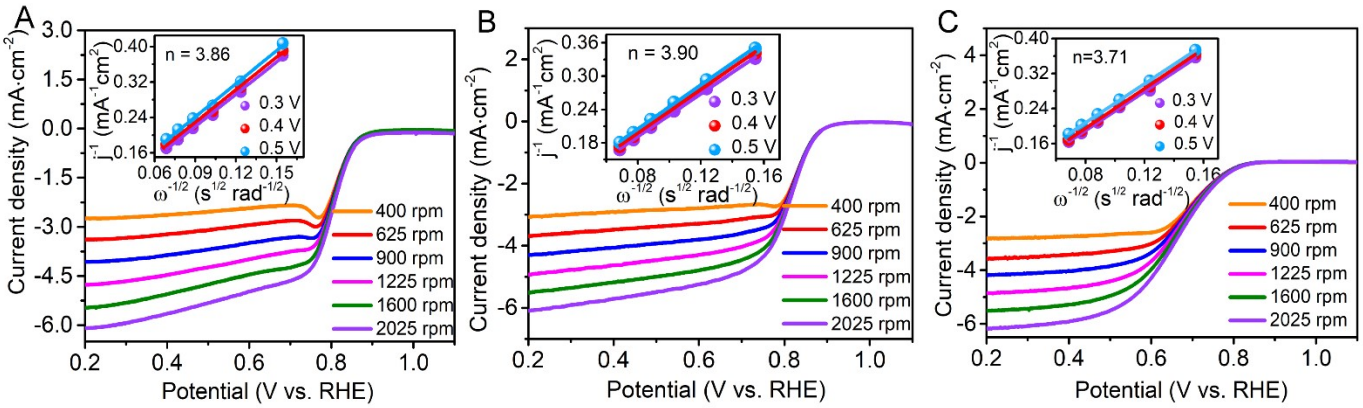

Fig. S18 LSV polarization curves of the Fe_{SA}/Fe_{AC}-NC 800 (A), Fe_{SA}/Fe_{AC}-NC 900 (B) and Fe_{SA}/Fe_{AC}-NC 1000 (C) catalyst in an O_2-saturated 0.1 M $HClO_4$ aqueous solution at a sweep rate of 5 mV s^{-1} with different rotation rates (400-2025 rpm) and the corresponding K-L plots (j^{-1} versus $\omega^{-1/2}$) at different potentials (inset).

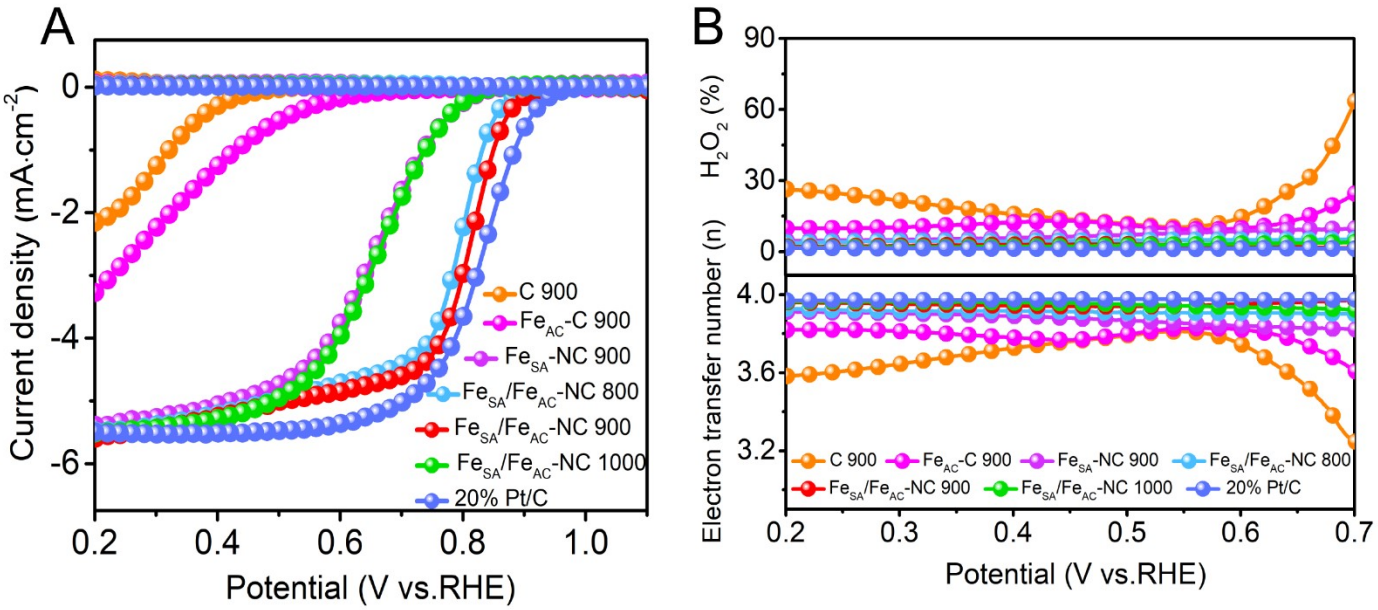

Fig. S19 A) Disk and ring current, B) electron transfer number (n) and H_2O_2 yield for various catalysts at 1600 rpm in acid media.

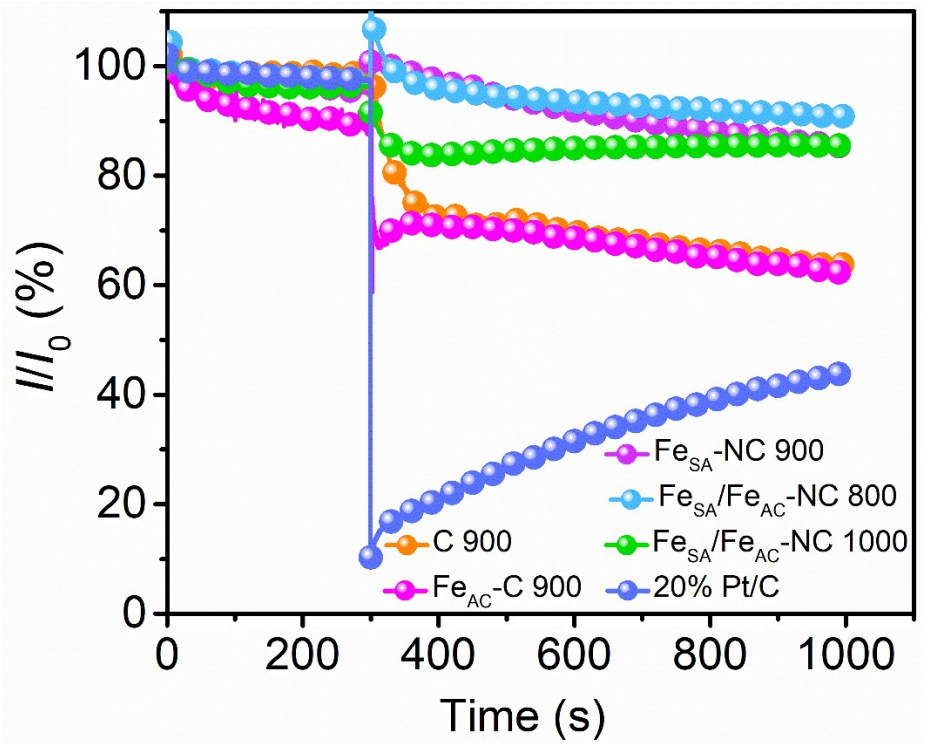

Fig. S20 *I-t* CA responses for various catalysts at 0.6 V and 1600 rpm with 3M methanol addition at around 300s in 0.1 M $HClO_4$. I_0 defined the initial current.

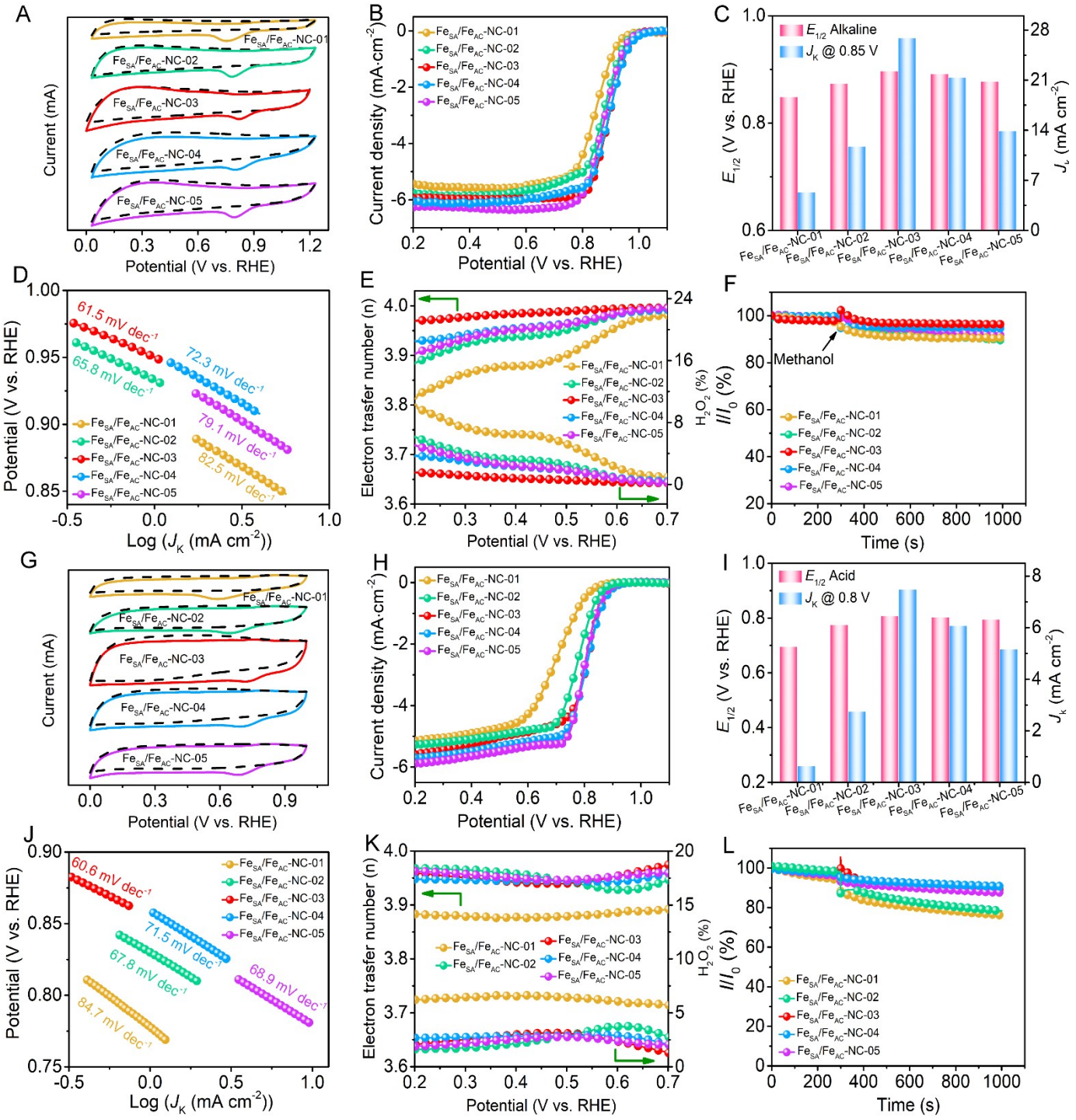

Fig. S21 Electrocatalytic ORR performance of Fe$_{SA}$/Fe$_{AC}$-NCs. Alkaline electrolyte. A) CV curves. B) LSV curves. C) Summary of $E_{1/2}$ and J_k at 0.85 V. D) Tafel slopes. E) n and H_2O_2 yield. F) Crossover tolerance. **Acid electrolyte.** G) CV curves. H) LSV curves. I) Summary of $E_{1/2}$ and J_k at 0.80 V. J) Tafel slopes. K) n and H_2O_2 yield. L) Crossover tolerance.

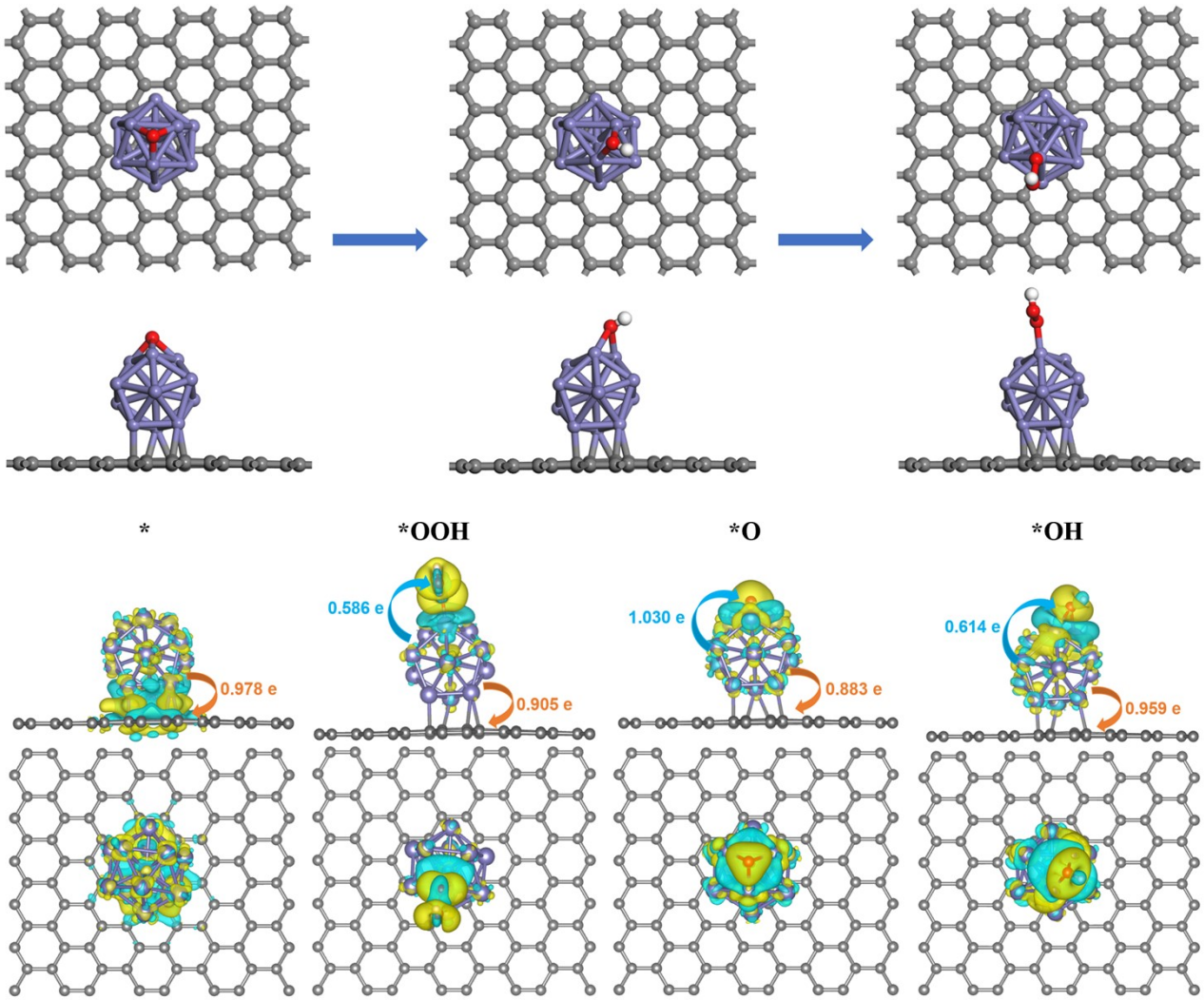

Fig. S22 The relaxed structures of oxygenous intermediates (*OOH, *O, and *OH) on the Fe_{AC}/C model and the corresponding Bader charge are labeled with an isosurface of 0.0015 e $Bohr^{-3}$ by DFT calculation. The orange arrows represent the charge transfer from the Fe cluster to the carbon substrate, while the blue arrows represent the charge transfer from the Fe cluster to the oxygenous intermediates. The yellow region represents the charge accumulation, while the cyan region represents the charge depletion.

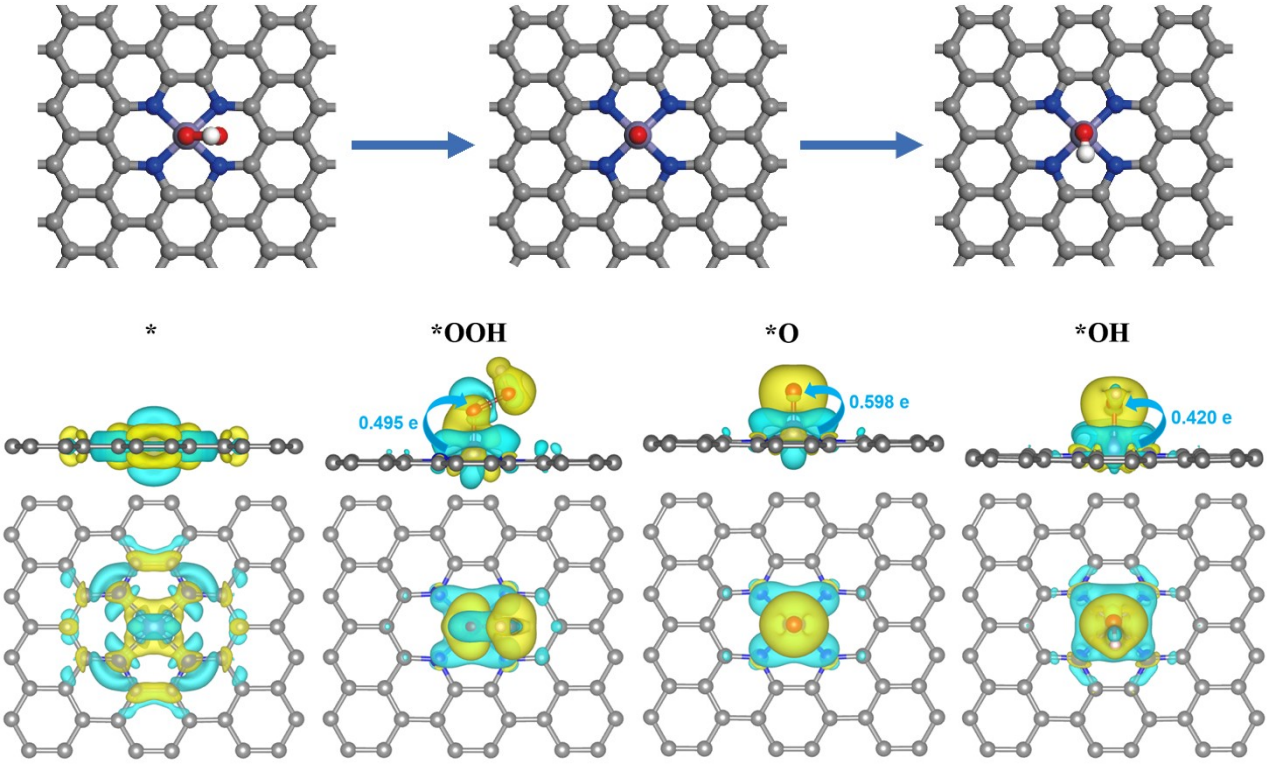

Fig. S23 The relaxed structures of oxygenous intermediates (*OOH, *O, and *OH) on the Fe_{SA}/C model and the corresponding Bader charge are labeled with an isosurface of 0.0015 e $Bohr^{-3}$ by DFT calculation. The blue arrows represent the charge transfer from the FeN_4 site to the oxygenous intermediates. The yellow region represents the charge accumulation, while the cyan region represents the charge depletion.

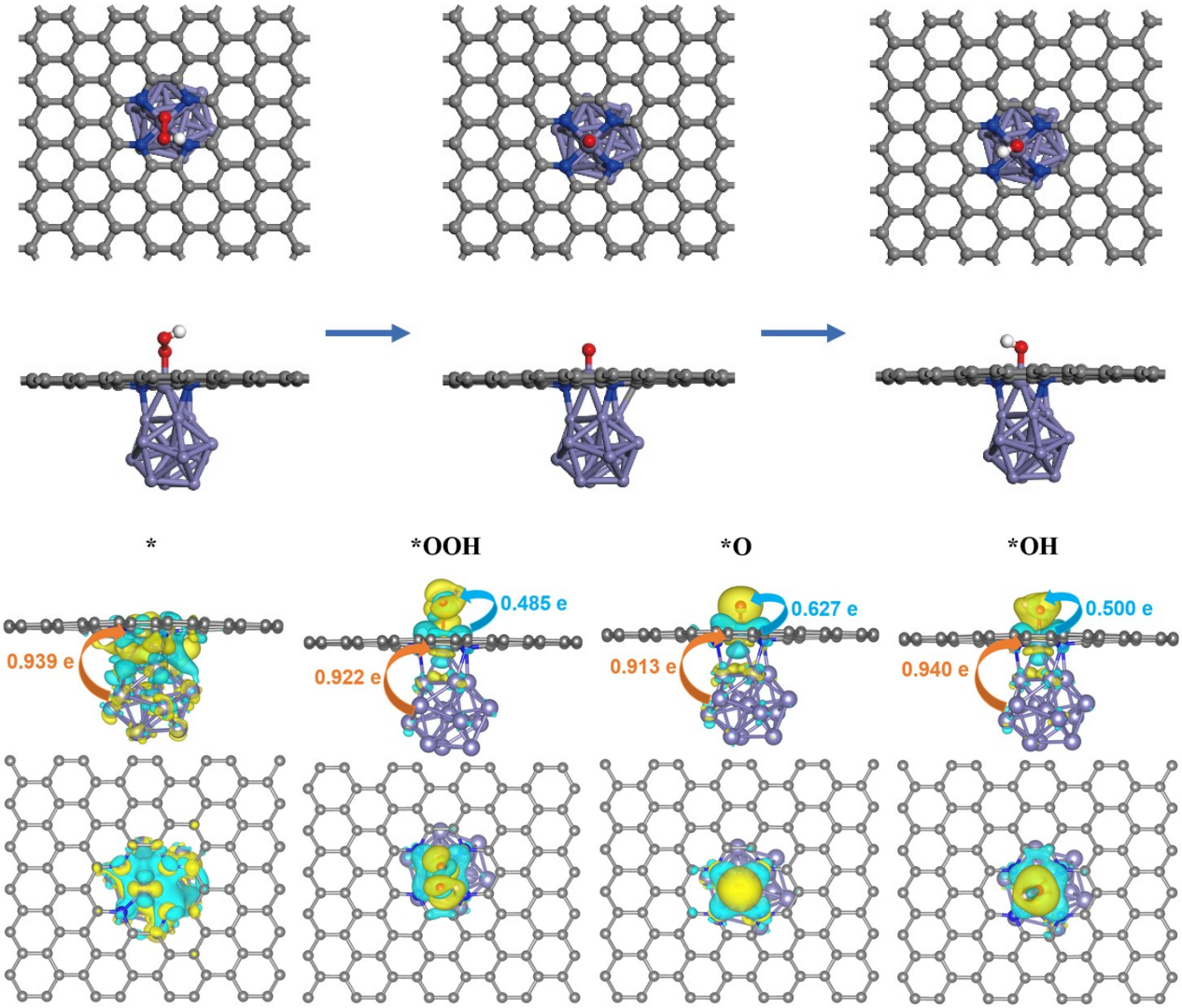

Fig. S24 The relaxed structures of oxygenous intermediates (*OOH, *O, and *OH) on the Fe_{SA}/C-Fe_{AC} model and the corresponding Bader charge are labeled with an isosurface of 0.0015 e $Bohr^{-3}$ by DFT calculation. The orange arrows represent the charge transfer from the Fe cluster to the FeN_4 site, while the blue arrows represent the charge transfer from the FeN_4 site to the oxygenous intermediates. The yellow region represents the charge accumulation, while the cyan region represents the charge depletion.

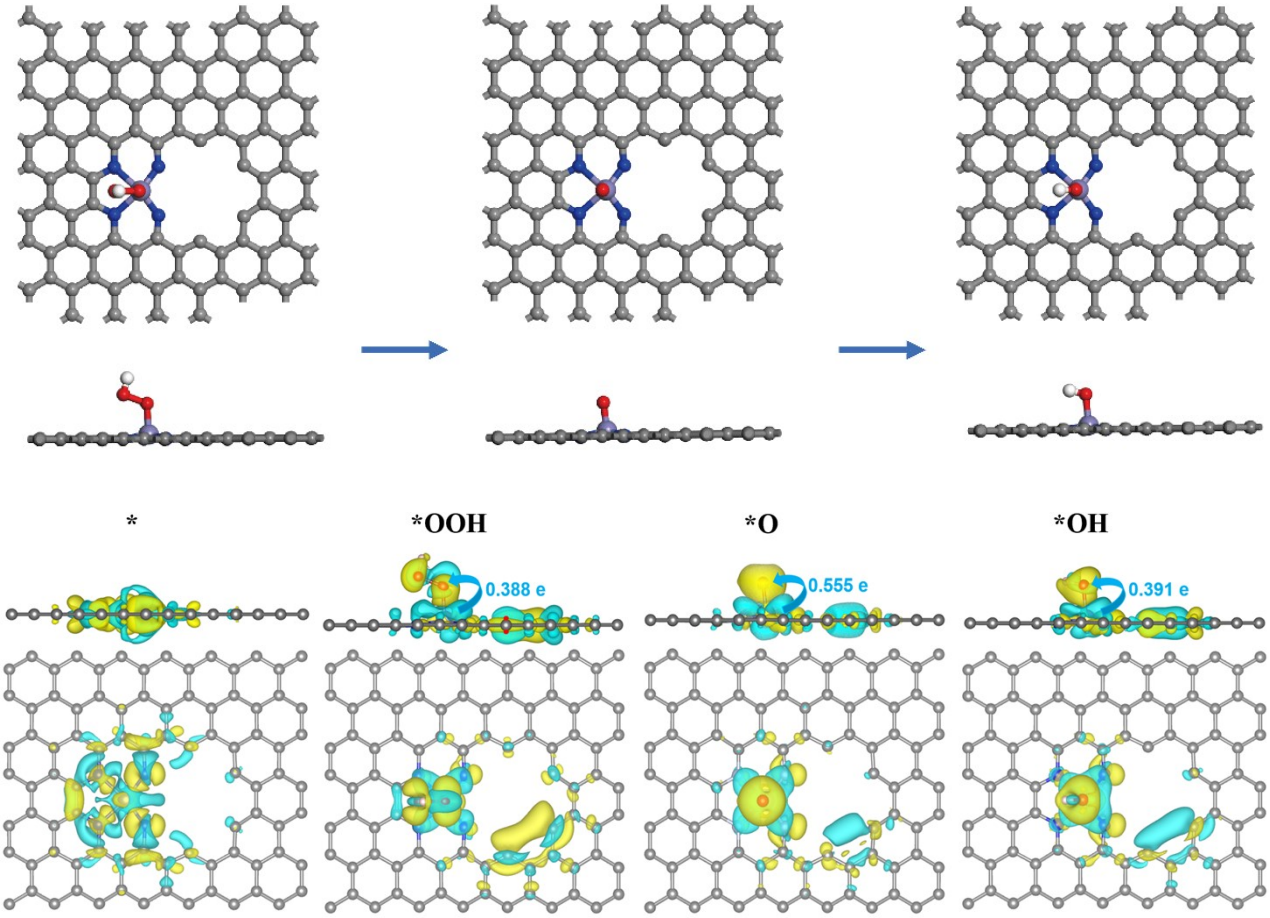

Fig. S25 The relaxed structures of oxygenous intermediates (*OOH, *O, and *OH) on the Fe_{SA}/C-Pore model and the corresponding Bader charge are labeled with an isosurface of 0.0015 e $Bohr^{-3}$ by DFT calculation. The blue arrows represent the charge transfer from the FeN_4 site to the oxygenous intermediates. The yellow region represents the charge accumulation, while the cyan region represents the charge depletion.

Fig. S26 Photograph of the 20% Pt/C-based Zn-air battery with an open circuit voltage of 1.39 V.

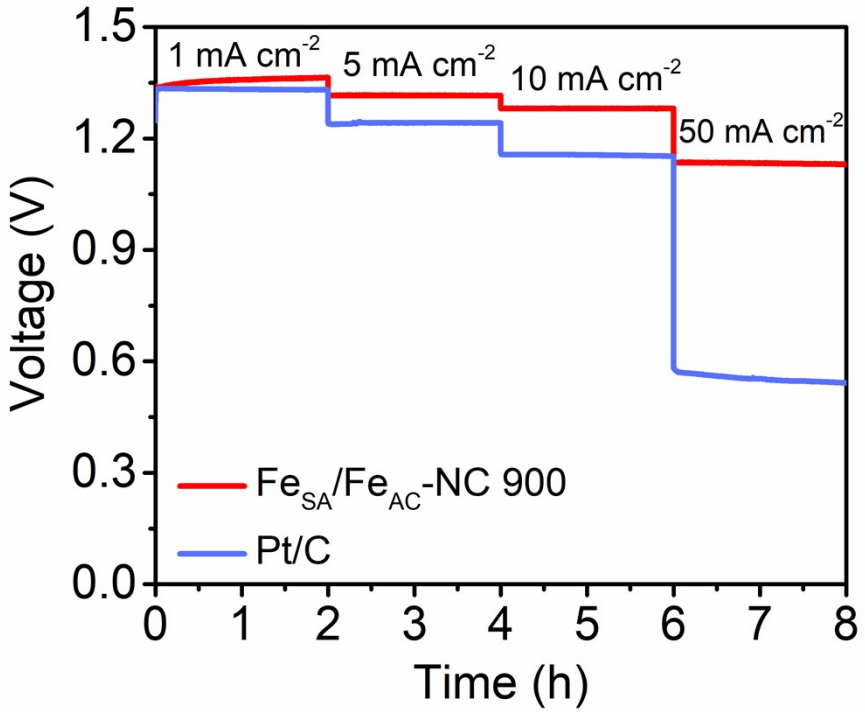

Fig. S27 Discharge profiles of the Zn-air batteries using Fe_{SA}/Fe_{AC}-NC 900 and 20% Pt/C as the air catalysts different current densities (1, 5, 10 and 50 mA cm^{-2})

Table S1 Elements contents of various catalysts from element analyzer and ICP-OES.

Catalysts	Elements contents (wt%)			
	C	H	N	Fe
C 900	82.38	1.16	-	-
Fe_{AC} -C 900	96.37	0.25	-	1.96
Fe_{SA}-NC 900	94.19	0.20	0.73	0.51
Fe_{SA}/Fe_{AC}-NC 800	74.28	2.01	2.44	3.19
Fe_{SA}/Fe_{AC}-NC 900	83.96	2.45	3.78	2.24
Fe_{SA}/Fe_{AC}-NC 1000	90.38	0.60	0.61	1.33

Table S2 BET results of the as-prepared samples.

Samples	Specific surface area (m^2 g^{-1})	Pore volume (cm^3 g^{-1})	Pore diameter (nm)
C 900	772.51	0.37	2.41
Fe_{AC}-C 900	200.77	0.39	7.75
Fe_{SA}-NC 900	262.54	0.38	7.36
Fe_{SA}/Fe_{AC}-NC 800	743.70	0.38	2.52
Fe_{SA}/Fe_{AC}-NC 900	968.32	0.52	2.36
Fe_{SA}/Fe_{AC}-NC 1000	359.62	0.40	4.84

Table S3 Comparison of the element contents of various catalysts obtained from XPS analysis.

Samples	C (at.%)	N (at.%)	O (at.%)	Fe (at.%)
C 900	91.82	-	8.18	-
Fe_{AC}-C 900	97.62	-	1.93	0.45
Fe_{SA}-NC 900	96.71	1.23	1.86	0.20
Fe_{SA}/Fe_{AC}-NC 800	90.79	3.19	5.60	0.42
Fe_{SA}/Fe_{AC}-NC 900	88.10	3.86	7.62	0.42
Fe_{SA}/Fe_{AC}-NC 1000	95.24	1.17	3.21	0.38

Table S4 Comparison of the nitrogen configurations of Fe_{SA}/Fe_{AC}-NC 800, Fe_{SA}/Fe_{AC}-NC 900 and Fe_{SA}/Fe_{AC}-NC 1000 catalysts.

Samples	Pyridinic-N (%)	Fe-N_x (%)	Pyrrolic-N (%)	Graphitic-N (%)	Oxidized N (%)
	~398.6 eV	~399.4 eV	~400.2 eV	~401.2 eV	~403.4 eV
Fe_{SA}/Fe_{AC}-NC 800	20.51	6.41	6.41	46.37	20.30
Fe_{SA}/Fe_{AC}-NC 900	21.26	9.54	10.26	47.21	11.73
Fe_{SA}/Fe_{AC}-NC 1000	11.41	9.49	7.55	53.83	17.72

Table S5 Fe K-edge fitting parameters.

Sample	shell	N	R (Å)	ΔE_0 (eV)	σ^2 (Å^2)	R factor
Fe foil	Fe-Fe	8.0	2.47	5.5	0.0054	0.005
	Fe-Fe	6.0	2.85		0.0071	
Fe_{SA}/Fe_{AC}-NC 900	Fe-N	4.1±0.4	2.01	-0.76	0.0089	0.016
	Fe-Fe1	0.5±0.007	2.50		0.0023	
	Fe-Fe2	3.1±0.5	3.03		0.0102	

Table S6 The ORR performance parameters of various samples tested in alkaline media.

Samples	E_p (V vs. RHE)	E_{onset} (V vs. RHE)	$E_{1/2}$ (V vs. RHE)	J_L (0.2 V, mA·cm^{-2})
C 900	0.63	0.79	0.72	3.29
Fe_{AC}-C 900	0.60	0.77	0.66	4.57
Fe_{SA}-NC 900	0.74	0.93	0.83	5.41
Fe_{SA}/Fe_{AC}-NC 800	0.81	0.98	0.89	5.65
Fe_{SA}/Fe_{AC}-NC 900	0.82	0.98	0.90	5.93
Fe_{SA}/Fe_{AC}-NC 1000	0.76	0.93	0.85	5.90
20% Pt/C	-	0.96	0.86	5.51

Table S7 Summary of reported ORR activity of PGM-free catalysts. All catalysts were estimated in an O_2-saturated 0.1 M KOH electrolyte.

Catalysts	E_{onset} (V vs. RHE)	$E_{1/2}$ (V vs. RHE)	J_k (mA cm^{-2})	Reference
Fe_{SA}/Fe_{AC}-NC 900	**0.98**	**0.90**	**26.90 at 0.85 V**	**This work**
Co/MnO@N,S-CNT/NFs	-	0.84	-	[1]
HLM/C	0.95	0.75	-	[2]
E-FeNC	-	0.875	7.95 at 0.85 V	[3]
Fe SACs	-	0.85	-	[4]
FeZ-CNS-900	0.963	0.881	24.10 at 0.85 V	[5]
Mo/C tubes	-	0.81	-	[6]
Fe(Fc)−N/S−C	0.991	0.872	-	[7]
0.14Co0.01Fe–CB	-	0.86	-	[8]
commercial Fe–N–C	-	0.846	-	[9]
FeNC-SN-2	0.982	0.890	1.99 at 0.90 V	[10]
Cu−N−C/GC	0.98	0.84	-	[11]

Table S8 The ORR performance parameters of various samples tested in acid media.

Samples	E_p (V vs. RHE)	E_{onset} (V vs. RHE)	$E_{1/2}$ (V vs. RHE)	J_L (0.2 V, mA·cm^{-2})
C 900	0.13	0.45	0.31	2.16
Fe_{AC}-C 900	0.18	0.61	0.36	3.28
Fe_{SA}-NC 900	0.54	0.80	0.65	5.37
Fe_{SA}/Fe_{AC}-NC 800	0.67	0.86	0.78	5.48
Fe_{SA}/Fe_{AC}-NC 900	0.73	0.90	0.80	5.61
Fe_{SA}/Fe_{AC}-NC 1000	0.54	0.80	0.66	5.51
20% Pt/C	-	0.93	0.83	5.49

Table S9 Summary of reported ORR activity of PGM-free catalysts. All catalysts were estimated in an O_2-saturated 0.1 M $HClO_4$ electrolyte.

Catalysts	E_{onset} (V vs. RHE)	$E_{1/2}$ (V vs. RHE)	J_k (mA cm^{-2})	Reference
Fe_{SA}/Fe_{AC}-NC 900	**0.89**	**0.80**	**7.48 at 0.80 V**	**This work**
HPFe-N-C	-	0.802	6.713 at 0.80 V	[12]
FeN_4Cl_1/NC	-	0.79	24 at 0.75 V	[13]
Ca-N, O/C	-	0.77	-	[14]
Mn–N–C–OAc-10-second	-	0.80	0.41 at 0.85 V	[15]
D-Fe SAC	-	0.78	-	[16]
Fe−C−N950	-	0.8	-	[17]
Fe-N/P-C-700	0.89	0.72	-	[18]
Fe/Zn-N-C	0.985	0.808	-	[19]
SnNC	-	~0.73	-	[20]
Fe/NC-NaCl	0.960	0.832	15.0 at 0.85 V	[21]

Table S10 The ORR performance parameters of samples with different Fe contents.

Catalysts	E_{onset}-alkaline/acid (V vs. RHE)	$E_{1/2}$-alkaline/acid (V vs. RHE)	J_k-alkaline (@0.85V) /acid (@0.80V) (mA cm^{-2})
Fe_{SA}/Fe_{AC}-NC-01	0.94/0.82	0.85/0.70	5.32/0.64
Fe_{SA}/Fe_{AC}-NC-02	0.96/0.86	0.87/0.77	11.75/2.75
Fe_{SA}/Fe_{AC}-NC-03	0.98/0.89	0.90/0.80	26.90/7.48
Fe_{SA}/Fe_{AC}-NC-04	0.98/0.89	0.89/0.79	21.38/6.08
Fe_{SA}/Fe_{AC}-NC-05	0.97/0.88	0.88/0.78	13.90/5.16

Table S11 Free energies of the catalyst model.

Free Energies (eV) \ Catalyst	Fe_{AC} [a)]/C	Fe_{SA}/C	Fe_{SA}/C- Fe_{AC}	Fe_{SA}/C-Pore	Fe_{SA}/C-Pore-Fe_{AC}
* [b)]	-973.006	-280.99	-957.98	-949.52	-1097.39
*O	-979.305	-287.05	-963.29	-954.73	-1103.03
*OH	-983.465	-291.28	-967.86	-959.31	-1107.40
*OOH	-987.237	-295.47	-972.12	-963.63	-1111.64

[a)] Fe cluster represents 13 iron atoms.

[b)] * denotes the Fe atom of FeN_4 active center for the Fe_{SA}/C, Fe_{SA}/C- Fe_{AC}, Fe_{SA}/C-Pore, Fe_{SA}/C-Pore-Fe_{AC}, respectively.

Table S12 The performance of primary Zn-air batteries using PGM-free electrocatalysts.

Catalysts	Peak power density ($mW\ cm^{-2}$)	Durability (h)	Reference
Fe_{SA}/Fe_{AC}-NC 900	**214.3**	**120**	**This work**
Mo/C tubes	197	50	[6]
Fe_{SA}-N/Cs-OAc	165	60	[22]
D-Co@NC	115.4	200	[23]
OAC	113	-	[24]
3D SAFe	156	80	[25]
$CoSe_2$@NC	137.1	166.7	[26]
Fe,Mn/N–C	160.8	81	[27]
FeN_4-Te_n	183	20	[28]
$Fe_{0.5}$Co@HOMNCP	134	120	[29]
pl-S-40	148.5	100	[30]
SAC-FeN-WPC	152	80	[31]
BTC-Co-O-Cu-BTA	200	50	[32]
1/CNT	132.9	~33.3	[33]
Sb SAC	184.6	-	[34]
Co@DMOF-900	158	200	[35]
Co@NCW	47.5	240	[36]
SAs-Fe/N-CNSs	157.03	-	[37]
CNT@SAC-Co/NCP	172	210	[38]
N-CoS_2YSSs	81	165	[39]
$C_{PANI–TA–Fe}$ Fe-SA-NC	~136.4	180	[40]

Section 2. References

1 Q. Zhou, S. Hou, Y. Cheng, R. Sun, W. Shen, R. Tian, J. Yang, H. Pang, L. Xu, K. Huang, Y. Tanga, *Appl. Catal. B: Environ.*, 2021, **295**, 120281.

2 X. Zhong, M. Oubla, X. Wang, Y. Huang, H. Zeng, S. Wang, K. Liu, J. Zhou, L. He, H. Zhong, N. Alonso-Vante, C.-W. Wang, W.-B. Wu, H.-J. Lin, C.-T. Chen, Z. Hu, Y. Huang, J. Ma, *Nat. Commun.*, 2021, **12** 3136.

3 R. Ma, G. Lin, Q. Ju, W. Tang, G. Chen, Z. Chen, Q. Liu, M. Yang, Y. Lu, J. Wang, *Appl. Catal. B: Environ.,* 2020*,* **265**, 118593.

4 Z. Jin, P. Li, Y. Meng, Z. Fang, D. Xiao, G. Yu, *Nat. Catal.*, 2021, **4**, 615.

5 G. Li, L. Pei, Y. Wu, B. Zhu, Q. Hu, H. Yang, Q. Zhang, J. Liu, C. He, *J. Mater. Chem. A*, 2019, **7**, 11223–11233.

6 Y. Zhao, Z. Zhang, L. Liu, Y. Wang, T. Wu, W. Qin, S. Liu, B. Jia, H. Wu, D. Zhang, X. Qu, G. Qi, E. P. Giannelis, M. Qin, S. Guo, *J. Am. Chem. Soc.*, 2022, **144** 20571−20581.

7 X. Li, X. Yang, L. Liu, H. Zhao, Y. Li, H. Zhu, Y. Chen, S. Guo, Y. Liu, Q. Tan, G. Wu, *ACS Catal.*, 2021, **11**, 7450-7459.

8 W. Zhu, Y. Pei, J. C. Douglin, J. Zhang, H. Zhao, J. Xue, Q. Wang, R. Li, Y. Qin, Y. Yin, D. R. Dekel, M. D. Guiver, *Appl. Catal. B: Environ.*, 2021, **299**, 120656.

9 H. Adabi, A. Shakouri, N. U. Hassan, J. R. Varcoe, B. Zulevi, A. Serov, J. R. Regalbuto, W. E. Mustain, *Nat. Energy*, 2021, **6**, 834-843.

10 C. Shao, L. Wu, H. Zhang, Q. Jiang, X. Xu, Y. Wang, S. Zhuang, H. Chu, L. Sun, J. Ye, B. Li, X. Wang, *Adv. Funct. Mater.*, 2021, **31**, 2100833.

11 G. Xing, M. Tong, P. Yu, L. Wang, G. Zhang, C. Tian, H. Fu, *Angew. Chem. Int. Ed.*, 2022, **61**, e202211098.

12 H. Xu, D. Wang, P. Yang, L. Du, X. Lu, R. Li, L. Liu, J. Zhang, M. An, *Appl. Catal. B: Environ.*, 2022, **305**, 121040.

13 L. Hu, C. Dai, L. Chen, Y. Zhu, Y. Hao, Q. Zhang, L. Gu, X. Feng, S. Yuan, L. Wang, B. Wang, *Angew. Chem. Int. Ed.*, 2021, 60, 27324–27329.

14 Z. Lin, H. Huang, L. Cheng, W. Hu, P. Xu, Y. Yang, J. Li, F. Gao, K. Yang, S. Liu, P. Jiang, W. Yan, S. Chen, C. Wang, H. Tong, M. Huang, W. Zheng, H. Wang, Q Chen, *Adv. Mater.*, 2021, **33**, 2107103.

15 Z. Kong, T. Liu, K. Hou, L. Guan, *J. Mater. Chem. A*, 2022, **10**, 2826–2834.

16 J. Yang, Z. Wang, C. Huang, Y. Zhang, Q. Zhang, C. Chen, J. Du, X. Zhou, Y. Zhang, H. Zhou, L. Wang, X. Zheng, L. Gu, L. Yang, Y. Wu, *Angew. Chem. Int. Ed.*, 2021, **60**, 22722 –22728.

17 T. Al-Zoubi, Y. Zhou, X. Yin, B. Janicek, C. Sun, C. E. Schulz, X. Zhang, A. A. Gewirth, P. Huang, P. Zelenay, H. Yang, *J. Am. Chem. Soc.*, 2020, **142**, 5477−5481.

18 K. Yuan, D. Lützenkirchen-Hecht, L. Li, L. Shuai, Y. Li, R. Cao, M. Qiu, X. Zhuang, M. K. H. Leung, Y. Chen, U. Scherf, *J. Am. Chem. Soc.*, 2020, **142**, 2404−2412.

19 H. Li, S. Di, P. Niu, S. Wang, J. Wang, L. Li, *Energy Environ. Sci.*, 2022, **15**, 1601-1610.

20 F. Luo, A. Roy, L. Silvioli, D. A. Cullen, A. Zitolo, M. T. Sougrati, I. C. Oguz, T. Mineva, D. Teschner, S. Wagner, J. Wen, F. Dionigi, U. I. Kramm, J. Rossmeisl, F. Jaouen, P. Strasser, *Nat. Mater.*, 2020, **19**, 1215–1223.

21 Q. Wang, Y. Yang, F. Sun, G. Chen, J. Wang, L. Peng, Wan. Chen, L. Shang, J. Zhao, D. Sun-Waterhouse, T. Zhang, G. I. N. Waterhouse, *Adv. Energy Mater.*, 2021, **11**, 2100219.

22 F. Kong, Y. Huang, M. Chen, G. Meng, H. Tian, Y. Chen, Z. Chang, C. Chen, W. Sun, X. Cui, J. Shi, *Appl. Catal. B: Environ.*, 2022, **317**, 120281.

23 F. Zhang, L. Chen, H. Yang, Y. Zhang, Y. Peng, X. Luo, A. Ahmad, N. Ramzan, Y. Xu, Y. Shi, *Chem. Eng. J.*, 2022, **431**, 133734.

24 L. Deng, L. Qiu, R. Hu, L. Yao, Z. Zheng, X. Ren, Y. Li, C. He, *Appl. Catal. B: Environ.*, 2022, **305**,

121058.

25 Y. Jiao, X. Gu, P. Zhai, Y. Wei, W. Liu, Q. Chen, Z. Yang, J. Zuo, L. Wang, T. Xu, Y. Gong, *Nano Lett.*, 2022, **22**, 7386−7393.

26 K. Ding, J. Hu, J. Luo, W. Jin, L. Zhao, L. Zheng, W. Yan, B. Weng, H. Hou, X. Ji, *Nano Energy*, 2022, **91**, 106675.

27 G. Yang, J. Zhu, P. Yuan, Y. Hu, G. Qu, B.-A. Lu, X. Xue, H. Yin, W. Cheng, J. Cheng, W. Xu, J. Li, J. Hu, S. Mu, J.-N. Zhang, *Nat. Commun.*, 2021, **12**, 1734.

28 B. Ji, J. Gou, Y. Zheng, X. Zhou, P. Kidkhunthod, Y. Wang, Q. Tang, Y. Tang, *Adv. Mater.*, 2022, **34**, 2202714.

29 W. Li, B. Liu, D. Liu, P. Guo, J. Liu, R. Wang, Y. Guo, X. Tu, H. Pan, D. Sun, F. Fang, R. Wu, *Adv. Mater.*, 2022, **34**, 2109605.

30 Z. Shao, Q. Zhu, Y. Sun, Y. Zhang, Y. Jiang, S. Deng, W. Zhang, K. Huang, S. Feng, *Adv. Mater.*, 2022, **34**, 2110172.

31 L. Zhong, C. Jiang, M. Zheng, X. Peng, T. Liu, S. Xi, X. Chi, Q. Zhang, L. Gu, S. Zhang, G. Shi, L. Zhang, K. Wu, Z. Chen, T. Li, M. Dahbi, J. Alami, K. Amine, J. Lu, *ACS Energy Lett.*, 2021, **6**, 3624−3633.

32 M. F. Sanad, A.R. Puente Santiago, S.A. Tolba, M.A. Ahsan, O. Fernandez-Delgado, M. Shawky Adly, E.M. Hashem, M. Mahrous Abodouh, M.S. El-Shall, S.T. Sreenivasan, N.K. Allam, L. Echegoyen, *J. Am. Chem. Soc.*, 2021, **143**, 4064-4073.

33 L. Xie, X. P. Zhang, B. Zhao, P. Li, J. Qi, X. Guo, B. Wang, H. Lei, W. Zhang, U.P. Apfel, R. Cao, *Angew. Chem. Int. Ed.*, 2021, **60**, 7576-7581.

34 T. Wang, X. Cao, H. Qin, L. Shang, S. Zheng, F. Fang, L. Jiao, *Angew. Chem. Int. Ed.*, 2021, 60, 21237-21241.

35 S. Yuan, J. Zhang, L. Hu, J. Li, S. Li, Y. Gao, Q. Zhang, L. Gu, W. Yang, X. Feng, B. Wang, *Angew.*

Chem. Int. Ed., 2021, **60**, 21685–21690.

36 W. Li, F. Wang, Z. Zhang, S. Min, *Appl. Catal. B: Environ.*, 2022, **137**, 121758.

37 X.-F. Gong, Y.-L. Zhang, L. Zhao, Y.-K. Dai, J.-J. Cai, B. Liu, P. Guo, Q.-Y. Zhou, I. Yagi, Z.-B. Wang, *J. Mater. Chem. A*, 2022, **10**, 5971–5980.

38 J.-C. Li, Y. Meng, L. Zhang, G. Li, Z. Shi, P.-X. Hou, C. Liu, H.-M. Cheng, M. Shao, *Adv. Funct. Mater.*, 2021, **31**, 2103360.

39 X. F. Lu, S. L. Zhang, E. Shangguan, P. Zhang, S. Gao, X. W. (David) Lou, *Adv. Sci.*, 2020, **7**, 2001178.

40 H. Li, K. Du, C. Xiang, P. An, X. Shu, Y. Dang, C. Wu, J. Wang, W. Du, J. Zhang, S. Li, H. Tian, S. Wang, H. Xia, *J. Mater. Chem. A*, 2020, **8**, 17136–17149.